


## Article

# Numerical Simulation of Liquid Sloshing with Different Filling Levels Using OpenFOAM and Experimental Validation

Yichao Chen <sup>1</sup>  and Mi-An Xue <sup>1,2,\*</sup><sup>1</sup> College of Harbour Coastal and Offshore Engineering, Hohai University, Nanjing 210098, China; 17625972812@163.com<sup>2</sup> State Key Laboratory of Hydraulic Engineering Simulation and Safety, Tianjin University, Tianjin 300072, China

\* Correspondence: coexue@hhu.edu.cn

Received: 3 November 2018; Accepted: 23 November 2018; Published: 28 November 2018



**Abstract:** A series of numerical simulations were performed to explore the influences of filling level, excitation frequency and amplitude on liquid sloshing by using the open source Computational Fluid Dynamics toolbox OpenFOAM (Open Field Operation and Manipulation), which was fully validated by the experimental data. The results show that the dynamic impact pressure is proportional to the external excitation amplitude only in non-resonance frequency ranges. Pressure-frequency response curves demonstrate a transition process from a ‘soft-spring’ response to a ‘hard-spring’ response following the changes of the filling level. Such a transition process is found to be dominated by the ratio of the filling level to tank length and the critical value can be obtained. It is also found that wave breaking influences the period of sloshing wave in tanks and ultimately alters the resonance frequency from the linear theory.

**Keywords:** sloshing; filling level; pressure-frequency response; OpenFOAM; experiment

## 1. Introduction

Sloshing is a phenomenon commonly found in partially-filled liquid storage vessels, such as liquid cargo tanks and fuel tanks, in motion. Violent sloshing may result in serious structural damages to the liquid-tank or even overturn the liquid cargo ship. Thus, a reliable prediction of the sloshing is crucial for the design and deployment of such structures. For this purpose, theoretical analyses, physical experiments, and numerical simulations are commonly utilized.

As a pioneer, Moiseev [1] developed a nonlinear analytical solution for the sloshing problem by using the approximations and modal methods combined with the potential flow theory. Based on Moiseev theory, Faltinsen [2] developed a third-order steady-state solution for the liquid sloshing in a 2D rectangular tank under the swaying and rolling excitations. Faltinsen [3,4] also established nonlinear analytical solutions for liquid sloshing in a rectangular tank by using the multimodal approach. Ikeda and Nakagawa [5] studied liquid sloshing in a rectangular tank under a horizontal excitation using the potential flow theory and analyzed the influence of fluid sloshing on the nonlinear vibration of the structure. However, the theoretical analysis approach may lead to unreliable predictions when complex physical phenomena such as wave breaking and slamming occur due to their fundamental assumption of the potential flow.

Physical experiments are considered an accurate approach and have been widely used to investigate liquid sloshing particularly with a focus on the prediction of the impact pressure. Pistani and Thiagarajan [6] conducted a series of sloshing experiments to accurately measure the high pressure

generated during the impacts of the fluid. Xue et al. [7] experimentally investigated the effectiveness of baffles on reducing the sloshing pressure. Kalinichenko and Sekerzh-Zenkovich [8] experimentally studied the relationship between the maximum wave height and the Faraday wave frequency and analyzed the crushing mechanisms of several types of sloshing waves, the broken form and jet flow formation of Faraday waves under vertical excitations. In their study, the attenuation coefficients of different modal waveforms and the relationship between wave breaking and frequency were also obtained. Xue et al. [9] designed and built a liquid sloshing experimental rig driven by a wave-maker to study liquid sloshing problems in a rectangular tank with perforated baffles. Their results showed that the perforated baffle with a suitable orifice size is an effective baffle arrangement for reducing the sloshing amplitude at higher excitation frequencies. Cai et al. [10] conducted an experimental study on the resonance frequency and maximum impact pressure in Liquefied Natural Gas (LNG) carriers. Generally speaking, the experimental studies have made a significant contribution to advance the knowledge and to explore physics, but they are relatively expensive and are subjected to certain limitations, e.g. the scaling problem and difficulties on measuring the temporal-spatial variations of physical quantities.

Numerical simulations are now a popular approach for studying liquid sloshing. Xue et al. [11] developed a finite difference model for solving the Navier-Stokes (NS) equation with a turbulence model being incorporated to investigate the viscous liquid sloshing-wave interaction with baffles in a tank. Liu and Lin [12] numerically studied 3D non-linear liquid sloshing with broken free surfaces. In their model, the large-eddy-simulation (LES) approach is adopted to account for the effect of turbulence by using the Smagorinsky sub-grid scale (SGS) closure model. Buldakov [13] considered a 2D sloshing problem in a rectangular tank under horizontal and vertical excitation using a Lagrangian model. Xue et al. [14] modelled the liquid sloshing in a baffled-tank using a time domain NS solver. Kim [15] investigated 2D and 3D liquid sloshing in containers by solving the NS model using the solution algorithm “Synchronized OverLap-and-Add” (SOLA) scheme, in which the free surface profile is assumed to be a single-valued function. Ramaswamy et al. [16] studied 2D viscous flow sloshing by using the Lagrange-finite element method. Oxtoby [17] described a semi-implicit volume-of-fluid (VOF) free surface modelling methodology for flow problems involving violent free-surface motions. Kishev et al. [18] developed a new Computational Fluid Dynamics (CFD) simulation approach based on the constraint interpolation profile (CIP) method to tackle the violent sloshing problem. Chen and Zong [19] presented an improved Smoothed Particle Hydrodynamics (SPH) model for the liquid sloshing and discussed the relationship between the pressure amplitude and the excitation frequency. Xue and Lin [20] studied the effects of ring baffles on reducing the violent liquid sloshing using their 3D free surface turbulent model and discussed the damping mechanism of the ring baffle. Kim [21] applied both the finite-difference method and SPH model to the simulation of violent sloshing. Jin and Lin [22] investigated the viscous effects on liquid sloshing under external excitations and found that the peak value of the maximal pressure occurs near the natural frequency with a very small (less than 3% of natural frequency) phase shift due to the wave nonlinearity. Recently, the open source CFD toolbox, OpenFOAM, has also been used to study the sloshing and coupling effects with ship motion and other problems [23–25].

Although a great deal of effort has been devoted to studying the liquid sloshing using the above-mentioned three approaches, challenges and research gaps still exist, especially for violent liquid sloshing, in which the nonlinearities due to the breaking waves and hydraulic jump in a shallow water condition may invalid the analytical solutions. One specific issue is the occurrence of the resonance, which normally leads to the possible highest pressure, for the liquid sloshing in a tank with widely-ranged filling levels and large excitation amplitudes. This paper aims to contribute to this issue using a systematic numerical investigation using OpenFOAM with the aid of experimental studies. The filling level, excitation amplitudes, and frequencies are considered as the main variables in the investigations.

## 2. Numerical Model

This study employs the InterDyMFoam module in the OpenFOAM, which is a two-phase NS solver for incompressible, isothermal immiscible fluids with optional mesh motion and mesh topology changes including adaptive re-meshing. The interface capturing approach used in this module is the volume of fluid (VOF) based on the phase-fraction. The continuity equation, momentum equation, and phase equation are, respectively, as follows.

$$\frac{\partial \rho}{\partial t} + \nabla \cdot (\rho \mathbf{U}) = 0 \quad (1)$$

$$\frac{\partial \rho \mathbf{U}}{\partial t} + \nabla \cdot (\rho \mathbf{U} \mathbf{U}) - \nabla \cdot \boldsymbol{\tau} = C \kappa \nabla \alpha - g \mathbf{h} \nabla \rho - \nabla p_{rgh} \quad (2)$$

$$\frac{D\alpha}{Dt} = \frac{\partial \alpha}{\partial t} + \nabla \cdot (\alpha \mathbf{U}) = 0 \quad (3)$$

where  $\rho$  is the density,  $\mathbf{U}$  is the fluid velocity vector,  $\boldsymbol{\tau}$  is the shear stress,  $C$  is the surface tension coefficient which is set to 0 in the current investigation,  $\kappa$  is the interface curvature,  $\alpha$  is the volume fraction,  $g$  is the acceleration of gravity,  $\mathbf{h}$  is the position vector of the mesh centre measured from the coordinates origin,  $p_{rgh}$  is the dynamic pressure. The fluid density  $\rho$  and the viscosity coefficient  $\mu$  are respectively calculated by densities ( $\rho_1, \rho_2$ ) and viscosity ( $\mu_1, \mu_2$ ) of two fluids using the volume fraction  $\alpha$ ,

$$\begin{aligned} \rho &= \alpha \rho_1 + (1 - \alpha) \times \rho_2 \\ \mu &= \alpha \mu_1 + (1 - \alpha) \times \mu_2 \end{aligned} \quad (4)$$

OpenFOAM uses the Finite Volume Method to discretize its governing equations. A first-order implicit Euler discretization scheme is used for dealing with the time derivative terms, e.g.,  $\partial \mathbf{U} / \partial t$  and  $\partial \alpha / \partial t$ . The Gauss linear discretization scheme is selected for gradient estimation, e.g.,  $\nabla \cdot \mathbf{U}$ . Gauss linear corrected is considered for laplacian schemes such as  $\nabla p_{rgh}$ ,  $\nabla \rho$ . With regard to the divergence terms such as  $\nabla \cdot (\mathbf{U} \mathbf{U})$  and  $\nabla \cdot (\mathbf{U} \alpha)$ , the van Leer scheme is used. The PIMPLE algorithm, which is a combination of PISO (Pressure Implicit with Splitting of Operator) and SIMPLE (Semi-Implicit Method for Pressure-Linked Equations), is used for the velocity-pressure decoupling. More details of the InterDyMFoam can be found in the OpenFOAM website or other references. These will not be repeated here, only the solution process of the InterDyMFoam is illustrated in Figure 1 for completeness.

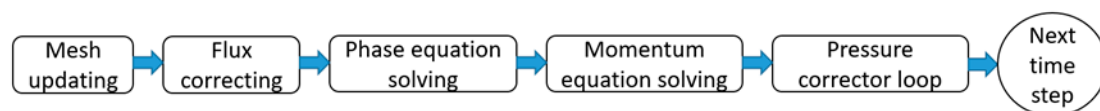
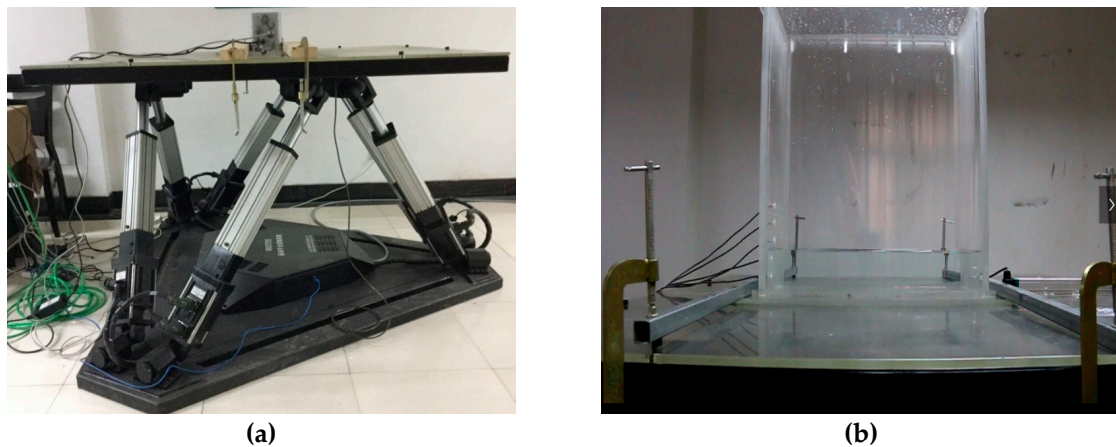


Figure 1. The flow chart of the solution.

## 3. Experimental Setup

For the purpose of validating the numerical model, as well as exploring detailed physics associated with the liquid sloshing, a series of experiments are carried out in the Laboratory of Vibration Test and Liquid Sloshing at the Hohai University, China. A six-degree of freedom (DoF) motion simulation platform, which is commonly known as a hexapod and is able to perform six-DoF motions regularly or randomly according to an appropriate input of time histories, is utilized to generate the forced motions of the liquid tank, as shown in Figure 2. The tank used in the experiments is a rectangular tank made of plexiglass with an 8-mm thickness. The internal dimensions of the rectangular tank are  $L = 600$  mm in length,  $W = 300$  mm in width and  $H = 650$  mm in height. A horizontal sinusoidal motion  $x = -A \sin \omega t$  is assigned to the rectangular tank. The amplitude and frequency of the motion can be set up through a control computer. The displacement of the motion platform was recorded by a displacement sensor. Figure 3, which compares both the actual motion platform displacement and theoretical displacement, indicates that the experimental apparatus has high motion accuracy.



**Figure 2.** The experimental setup of liquid sloshing (a). The motion simulation platform, (b). The liquid tank.

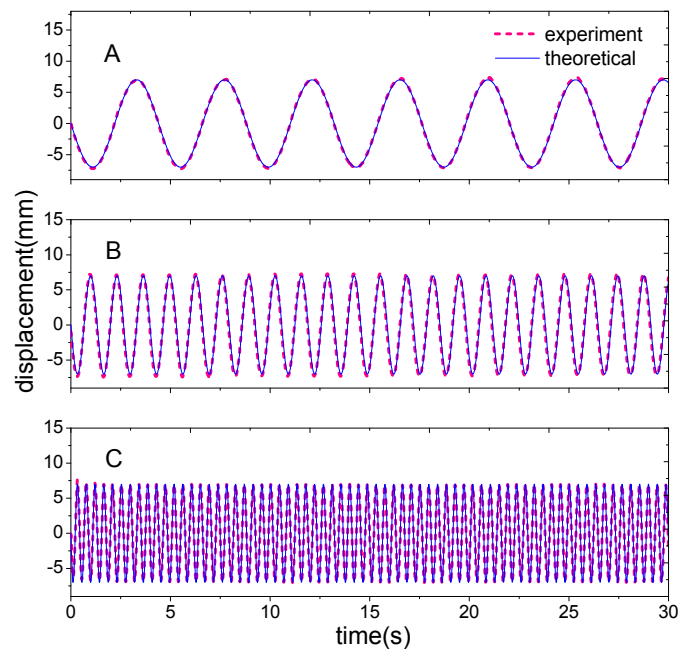


**Figure 3.** The comparisons of both the actual motion platform displacement and theoretical displacement (amplitude is 7 mm,  $\omega_A = 1.425$  rad/s,  $\omega_B = 4.749$  rad/s,  $\omega_C = 14.249$  rad/s).

In the experimental study, two filling levels, 13.8% and 30.8%, are considered. For measuring the dynamic impact pressure on the tank wall, five pressure sensors are embedded in the left wall, as shown in Figure 2. Their specific locations are illustrated in Figure 4. A camera was fixed in front of the rectangular tank to record the profile of the free surface.

With the assumption of potential flow theory, the natural frequencies can be analytically determined as [26]

$$\omega_n = \sqrt{g \frac{\pi n}{L} \tanh\left(\frac{\pi n}{L} h\right)}, \quad n = 1, 2, 3, \quad (5)$$

where  $n$  is the mode number and  $h$  is the filling level. According to Equation (5), the first-mode natural frequencies are  $\omega_1 = 4.749$  rad/s and  $\omega_1 = 6.333$  rad/s for the tank with the low (13.8%) and high (30.8%) filling level, respectively.

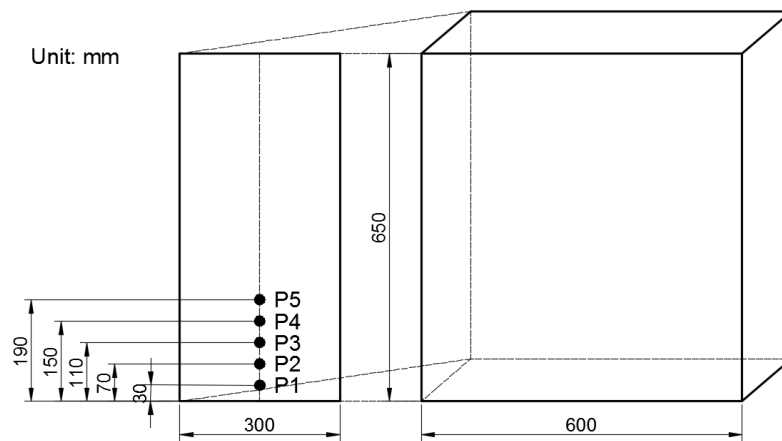


**Figure 4.** The inner dimension of the rectangular tank and the layout of five pressure sensors.

## 4. Model Validation

### 4.1. Mesh Convergence Test

Mesh convergence studies are performed to determine the mesh size used in the following simulations. The computational mesh consists of a uniform square grid. Three mesh sizes are considered in the tests. They are 2 mm, 5 mm and 8 mm, respectively. The model tank size is exactly the same as the experimental tank and the water depth is 90 mm (i.e., the low filling level in the experiment). The test parameters are chosen as  $A = 7$  mm and  $\omega = 4.749$  rad/s. The frequency is the same as the first mode natural frequency predicted using the linear theory (Equation (5)). Therefore, we expected to see a violent sloshing in the tank due to the resonance. If the mesh resolution leads to a convergent solution for this case, it shall be sufficient for other cases, especially non-resonance cases. The comparison of the pressure recorded at P1 in the cases with different mesh sizes is plotted in Figure 5. These results are all similar, although the result obtained by using the 8-mm mesh slightly differs from others. A mesh size of 5 mm is employed in the following studies. Furthermore, the time step size is automatically adjusted by the condition that the Courant number  $\leq 0.5$ .

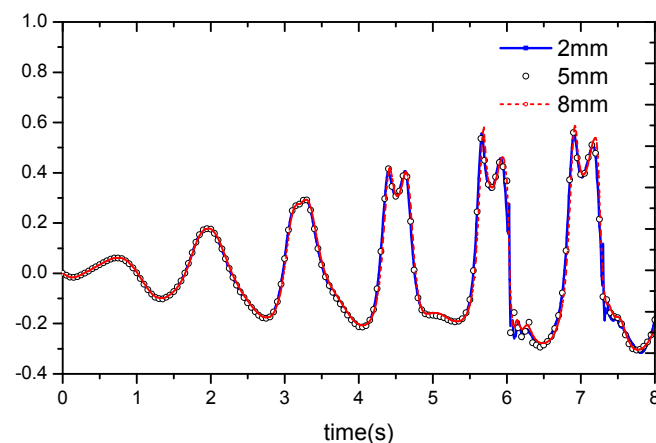


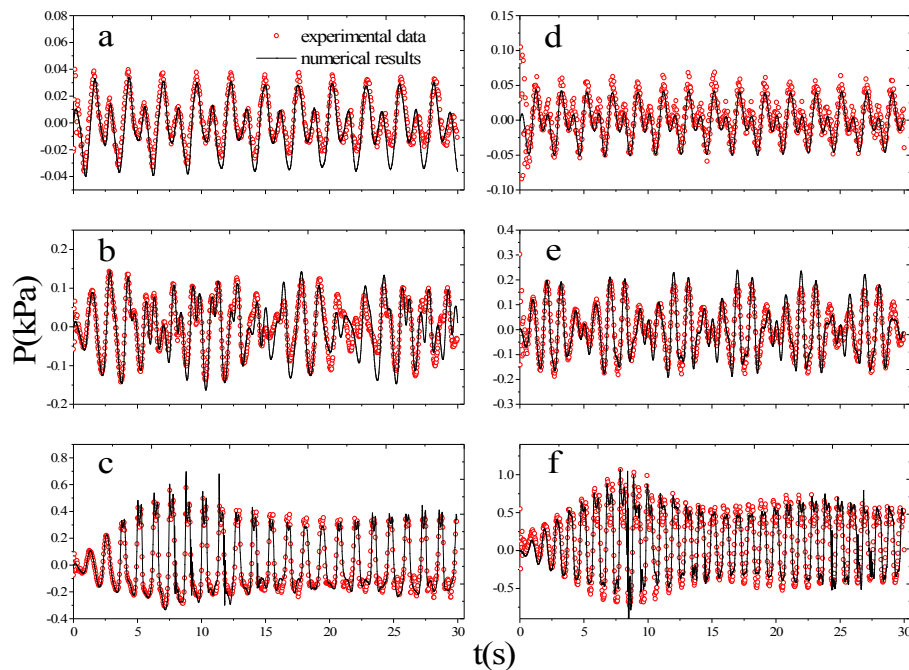
**Figure 5.** The comparisons of the pressure recorded at P1 in the cases with different mesh sizes.

### 4.2. Experimental Validation

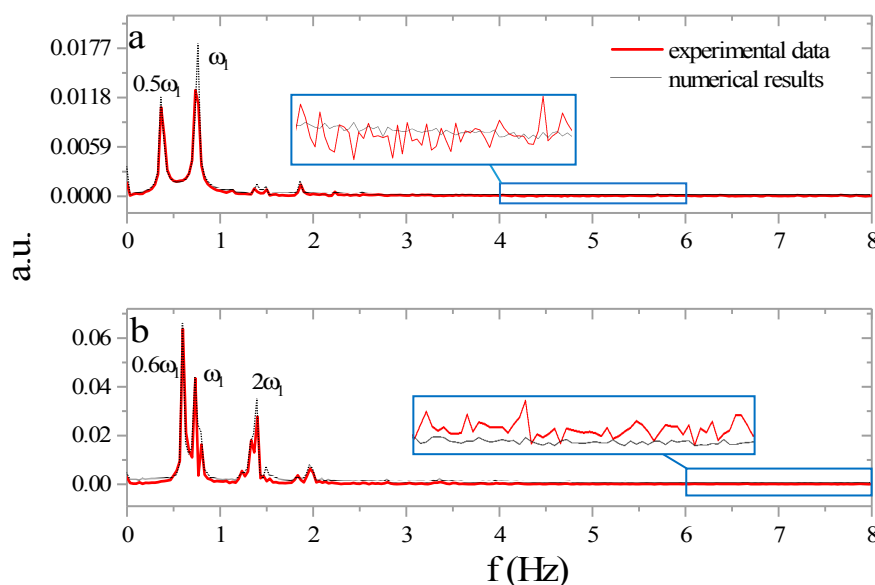
To validate the numerical model for the cases with different sloshing conditions, six sets of experimental data with two different filling levels and three different excitation frequencies are employed. The comparisons between the experimental data and the numerical results are illustrated in Figure 6, in which the red circles represent the experimental data and the black line represents the numerical results. Overall, the numerical results agree with the experimental data for the



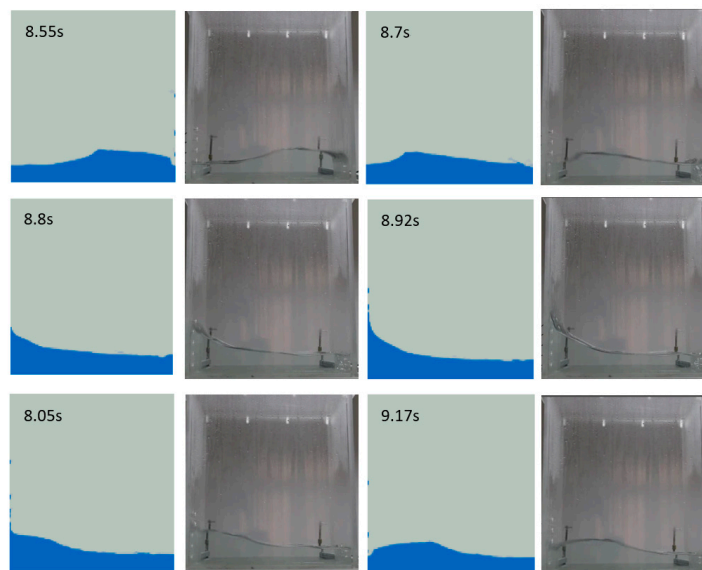
non-resonance (Figure 6a–d), near-resonance (Figure 6b–e), or fully-resonance (Figure 6c–f) conditions. It is noticed that the discrepancies between the numerical results and experimental results in the cases shown in Figure 6a,b become relatively more significant after  $t = 15$  s. Further analysis on the pressure spectra (Figure 7) suggests that the difference in Figure 6a is mainly caused by the fundamental pressure component (i.e.,  $\omega_1$ ) and the experimental data decays after  $t = 15$  s. For the case shown in Figure 6b, the spectra shown in Figure 7b further confirm a satisfactory agreement. In addition, the free surface profiles are also compared. Some results in the case with a resonance excitation are shown in Figure 8, which compares the wave profiles at six instants between 8.55 s and 9.17 s. A good match has been observed.



**Figure 6.** The model validation under different filling levels, external frequencies and the same amplitude of  $A = 7$  mm, (a)  $h = 90$  mm,  $\omega = 0.5 \omega_1$ , (b)  $h = 90$  mm,  $\omega = 0.8 \omega_1$ , (c)  $h = 90$  mm,  $\omega = \omega_1$ , (d)  $h = 200$  mm,  $\omega = 0.5 \omega_1$ , (e)  $h = 200$  mm,  $\omega = 0.8 \omega_1$ , (f)  $h = 200$  mm,  $\omega = \omega_1$ .

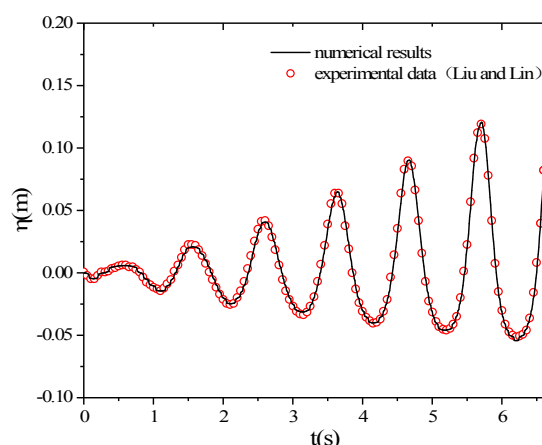


**Figure 7.** The Fast Fourier Transformation of the time history of the experimental and numerical pressure (amplitude is 7 mm,  $h = 90$  mm,  $\omega_a = 0.5 \omega_1$ ,  $\omega_b = 0.8 \omega_1$ ).

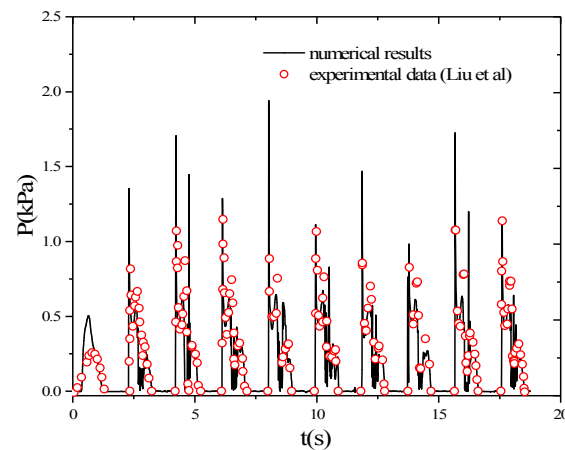


**Figure 8.** The numerical wave profile and experimental snapshot in six moments between 8.55 s and 9.17 s (amplitude is 7 mm,  $h = 90$  mm,  $\omega = \omega_1$ ).

For further validation, the experimental data in the literature are also used. The first case considered here is the 2D sloshing experiment carried out by Liu and Lin [12]. In this case, the tank dimensions are  $L = 570$  mm and  $H = 300$  mm. The water depth  $h$  is 150 mm. The tank undergoes a sinusoidal translation with an amplitude of 5 mm and the frequency of 6.0578 rad/s. The comparison of the surface elevation recorded near the left boundary (20 mm) between the numerical and experimental data is shown in Figure 9. Excellent agreement is observed. Another experiment was performed by Liu et al. [27], in which the 2D tank had a length of  $L = 900$  mm and a height of  $H = 508$  mm. The filling level  $h/H$  is 18.3%. The tank undergoes a sinusoidal rolling motion with motion amplitude of 4 degrees. The pressure recorded on the wall and at the mean water surface is used for comparison. The results are shown in Figure 10. Through such comparisons, one may agree that the present OpenFOAM modelling results in a satisfactory accuracy and is suitable for numerically simulating the sloshing problems.



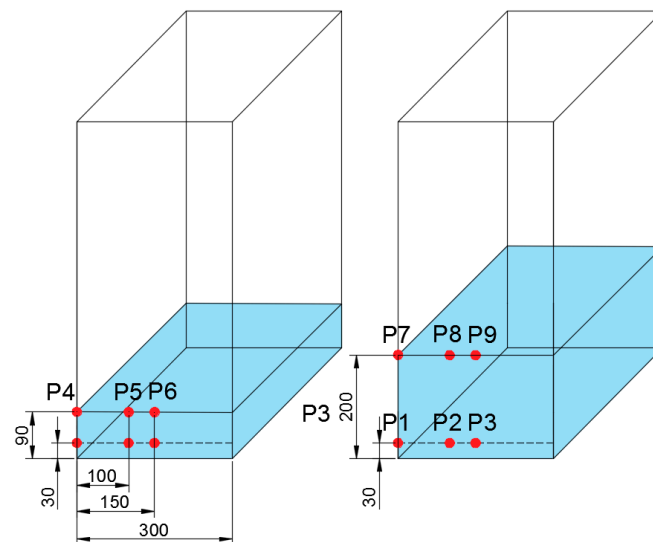
**Figure 9.** The validation of the free surface time history curve, experimental data (Liu and Lin) from [12].



**Figure 10.** The validation of the pressure history curve, experimental data (et al.) from [27].

#### 4.3. Three-Dimensional Results

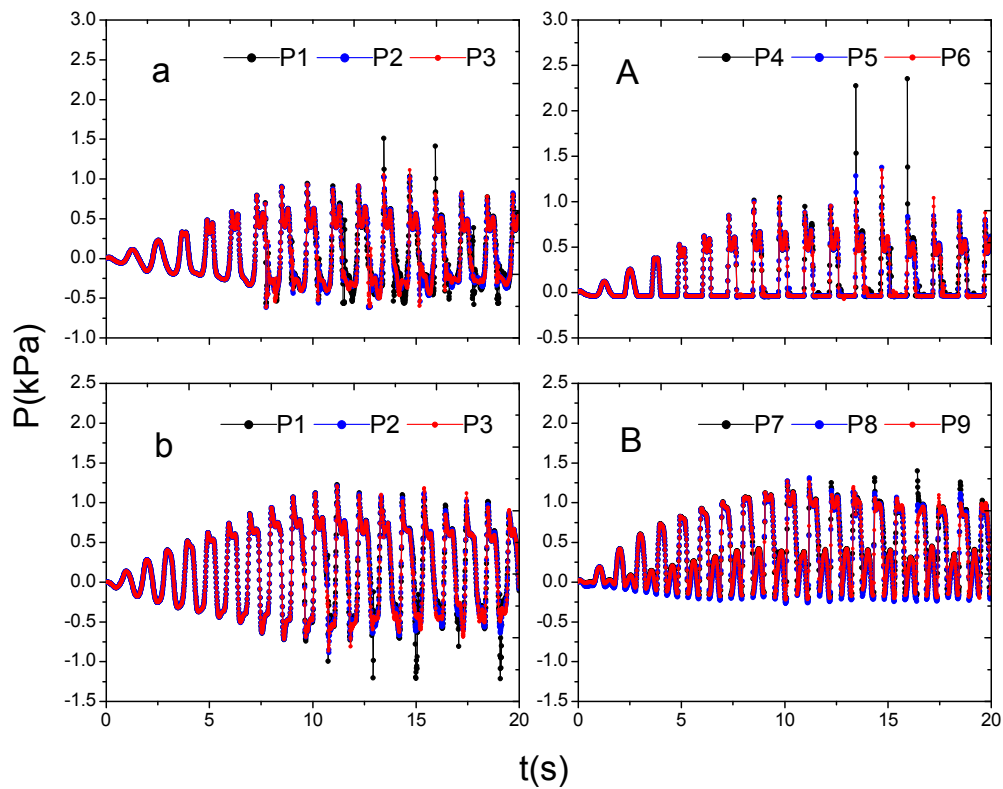
It is widely accepted that the single degree of freedom sloshing shown in Figures 7 and 8 can be simplified as 2D problems in the numerical simulation. However, in the cases under resonance conditions, the wave breaking occurs and the 3D effect may become important. To investigate the significance of the 3D effect, corresponding 3D numerical investigations are carried out. The numerical results by both the 2D model and the 3D model are compared with the experimental data to shed light on the 3D effect. In the 3D simulations, pressure probes are placed across the transverse direction (shown in Figure 11). Two cases subjected to resonant conditions are considered. These include Case A, where  $h = 90$  mm,  $f = 1.06 f_1$ , and  $A = 7$  mm, and Case B, in which  $h = 200$  mm,  $f = 0.96 f_1$ ,  $A = 7$  mm.



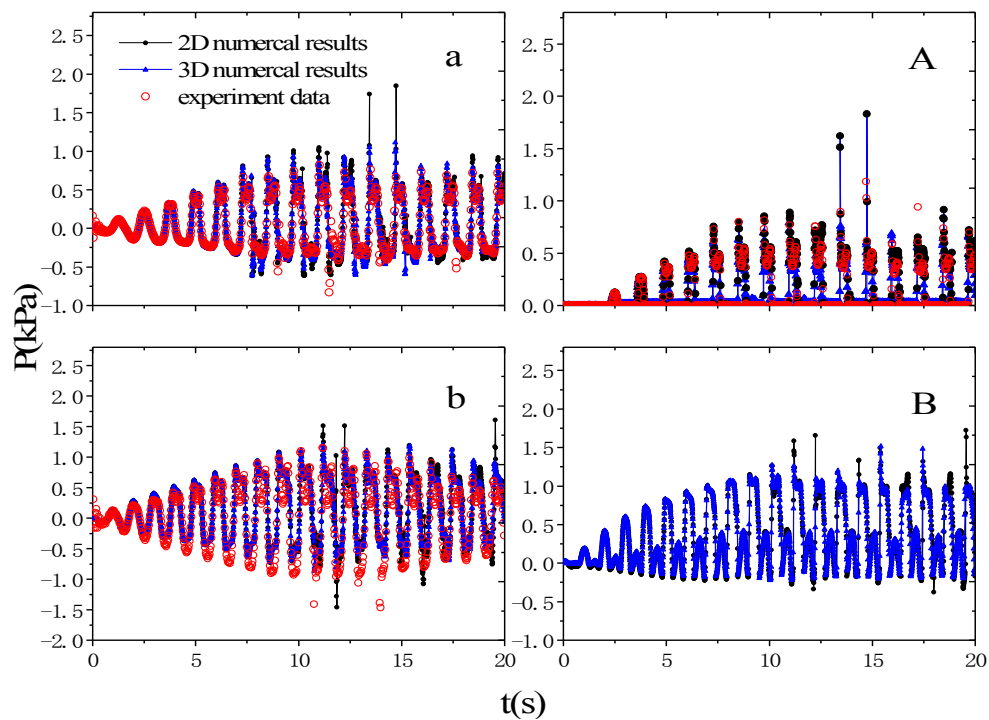
**Figure 11.** The locations of pressure probes.

Figure 12 compares the pressure-time histories at the probes located at the same height from the tank bottom in 3D numerical simulations but different transverse positions. As observed, the impact pressures at different transverse positions but the same height are largely the same, except the pressures at the corner of the tanks, e.g., P1, P4, and P7. Further comparison in Figure 13 shows that the 3D model leads to a slightly better prediction on the pressures on the corner points, compared to the 2D simulations. However, the superiority of the 3D model over the 2D model is not obvious in terms of the improvement of the computational accuracy. Considering the high computational demand of the 3D simulation, as demonstrated in Table 1, one may agree that the 2D model is preferable in terms of computational robustness for the problems concerned in this paper.





**Figure 12.** The comparison of impact pressure at different positions at the same height on the side wall. (a)  $h = 90$  mm,  $\omega = 1.06 \omega_1$ , pressure on the bottom, (A)  $h = 90$  mm,  $\omega = 1.06 \omega_1$ , pressure on the free surface, (b)  $h = 200$  mm,  $\omega = 0.96 \omega_1$ , pressure on the bottom, (B)  $h = 200$  mm,  $\omega = 0.96 \omega_1$ , pressure on the free surface.



**Figure 13.** The comparison of the 2D and 3D numerical results (a)  $h = 90$  mm,  $\omega = 1.06 \omega_1$ , pressure on the bottom, (A)  $h = 90$  mm,  $\omega = 1.06 \omega_1$ , pressure on the free surface, (b)  $h = 200$  mm,  $\omega = 0.96 \omega_1$ , pressure on the bottom, (B)  $h = 200$  mm,  $\omega = 0.96 \omega_1$ , pressure on the free surface.

**Table 1.** The comparison of parameters between the 2D model and 3D model.

	Two-dimensional Model	Three-dimensional Model
Mesh Size	5 × 5 mm	5 × 5 × 5 mm
Mesh Number	15,600	936,000
Computing Times	CPU:AMD Ryzen 7 1700X Eight-Core Processor 3.40 GHz no parallel 1962 s	394,971 s
Analysis of Result	In agreement with the experimental data; metimes there are large pressure peaks.	Match well with the experimental value

## 5. Results and Discussions

### 5.1. Effects of External Excitation Amplitudes

The excitation amplitude is an important factor that influences the intensity of the sloshing in the forced sloshing problem, and it reflects the input energy of the system. In this study, the influence of amplitude on the sloshing under different conditions will be discussed after a series of numerical studies being conducted. These cases are summarized in Table 2.

**Table 2.** The numerical case parameters.

Case	h/L	$\omega_1$ (rad/s)	$\omega/\omega_1$	$\omega$	A(m)
Case 1	0.15	4.749	0.5	2.3745	0.001
Case 2			0.6	2.8494	
Case 3			0.7	3.3243	
Case 4			0.8	3.7992	
Case 5			0.9	4.2741	
Case 6			1	4.749	
Case 7	0.33	6.333	0.5	3.1665	0.007
Case 8			0.6	3.7998	0.01
Case 9			0.7	4.4331	0.02
Case 10			0.8	5.0664	
Case 11			0.9	5.6997	
Case 12			1	6.333	

Figure 14 displays the response curves of the maximum impact pressure vs. the amplitude of the forced motion at different combinations of the filling level and frequency. It is worth mentioning that the vertical coordinate represents the peak of impact pressure which, at P1, was non-dimensionalized based on water depth, density and gravity ( $P = P_0/\rho gh$ ,  $h$  is set as 0.2 m). Data obtained through physical model experiments (the amplitudes are 3 mm, 5 mm and 7 mm respectively) are also added to Figure 14 for validation. It can be noted that the impact pressure increases as the amplitude increases and that increase is basically linear in the non-resonance range. In order to further illustrate this relationship, Figure 15 shows the pressure-time histories in the cases with different excitation amplitudes. For the convenience of the comparison, the pressure results in the cases with  $A = 1$  mm multiplied by a scaling factor of 3 is able to be comparable with the corresponding results with  $A = 3$  mm. If two curves in Figure 15 match with each other (e.g., Figure 15a–d), the pressure is then linearly dependent on the motion amplitude; otherwise, the nonlinearity becomes more important (e.g., Figure 15e–f). This condition often occurs following the occurrence of wave resonance and breaking.

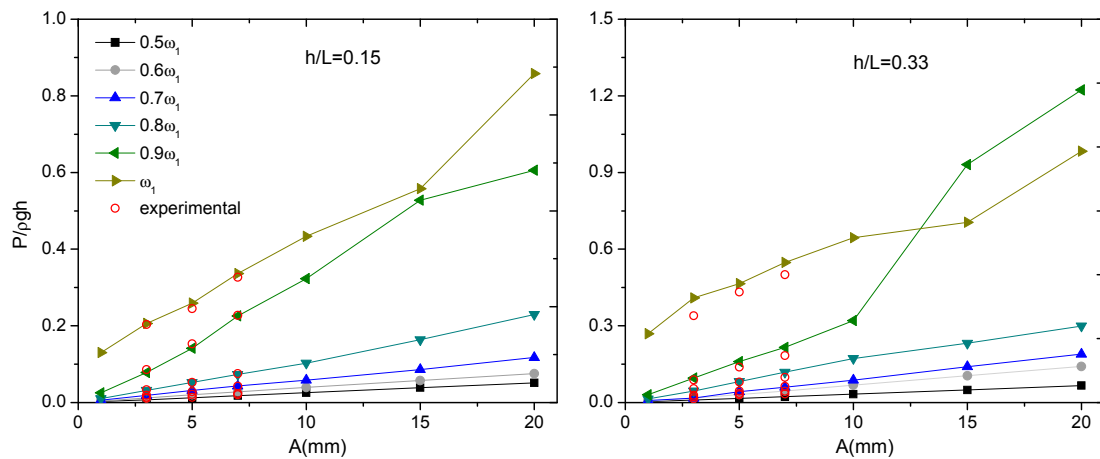


Figure 14. The amplitude–pressure response curve.

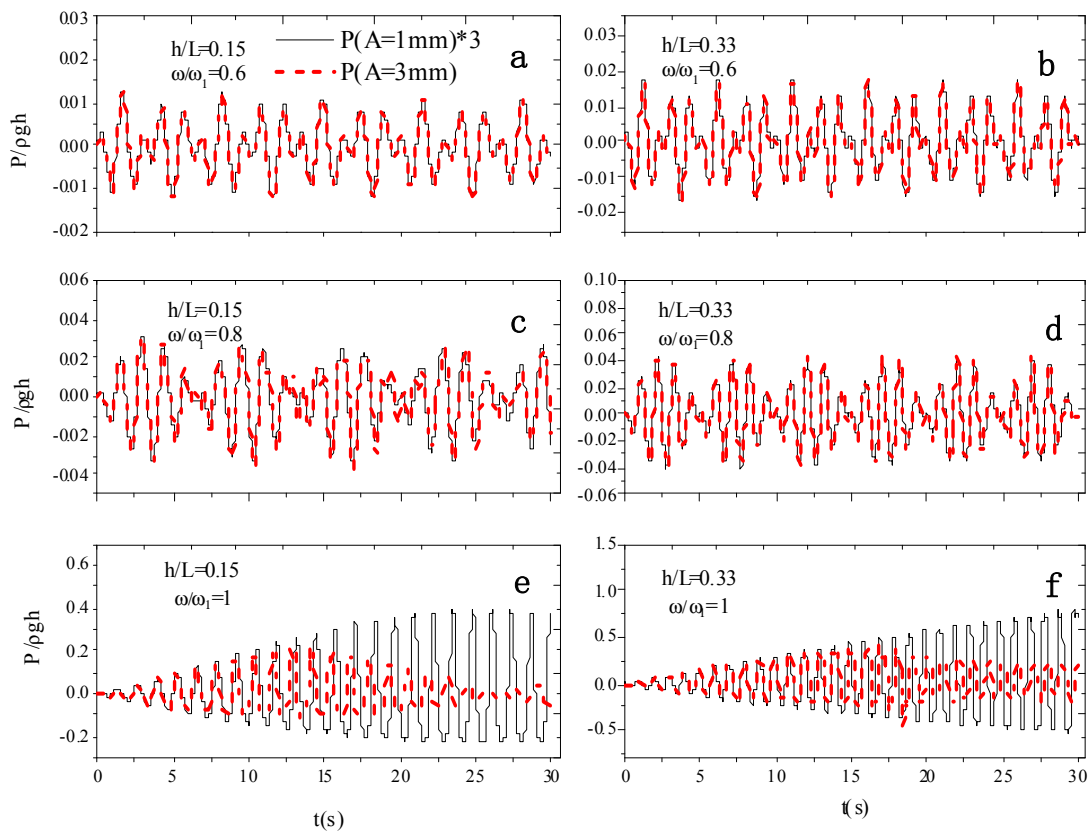


Figure 15. The comparison of pressure–time history curves at different amplitudes. (a)  $h/L = 0.15$ ,  $\omega = 0.6 \omega_1$ , (b)  $h/L = 0.33$ ,  $\omega = 0.6 \omega_1$ , (c)  $h/L = 0.15$ ,  $\omega = 0.8 \omega_1$ , (d)  $h/L = 0.33$ ,  $\omega = 0.8 \omega_1$ , (e)  $h/L = 0.15$ ,  $\omega = \omega_1$ , (f)  $h/L = 0.33$ ,  $\omega = \omega_1$ .

## 5.2. Resonant Hysteresis and Resonance in Advance

In the sloshing problem, the natural frequency of the tank can be computed using the analytical solution based on the potential flow theory Equation (5). However, the frequency leading to the maximum impact pressure is generally not consistent with the natural frequency due to the nonlinearity. The theory [28] has indicated the change in the resonant response from a so-called ‘hard-spring’ to ‘soft-spring’ behaviour as the filling level increases. Kobine’s [29] confirms the predicted change in the hysteresis behaviour with an increasing filling level. Based on these studies, this section mainly conducts studies to explore the mechanism of the resonant hysteresis.

A large number of numerical simulations are performed to explore the influence of the filling level on the response between the impact pressure of tank wall and external excitation frequency. The specific parameters of the cases are in Table 3. There are 10 filling levels, one amplitude of motion, 15 external excitation frequencies, 30 s of sloshing duration considered. In order to gather more stable and accurate pressure data, the pressure probe is set at the bottom of the tank wall which is away from the pressure impacts ( $h = 30$  mm).

**Table 3.** The numerical case parameters.

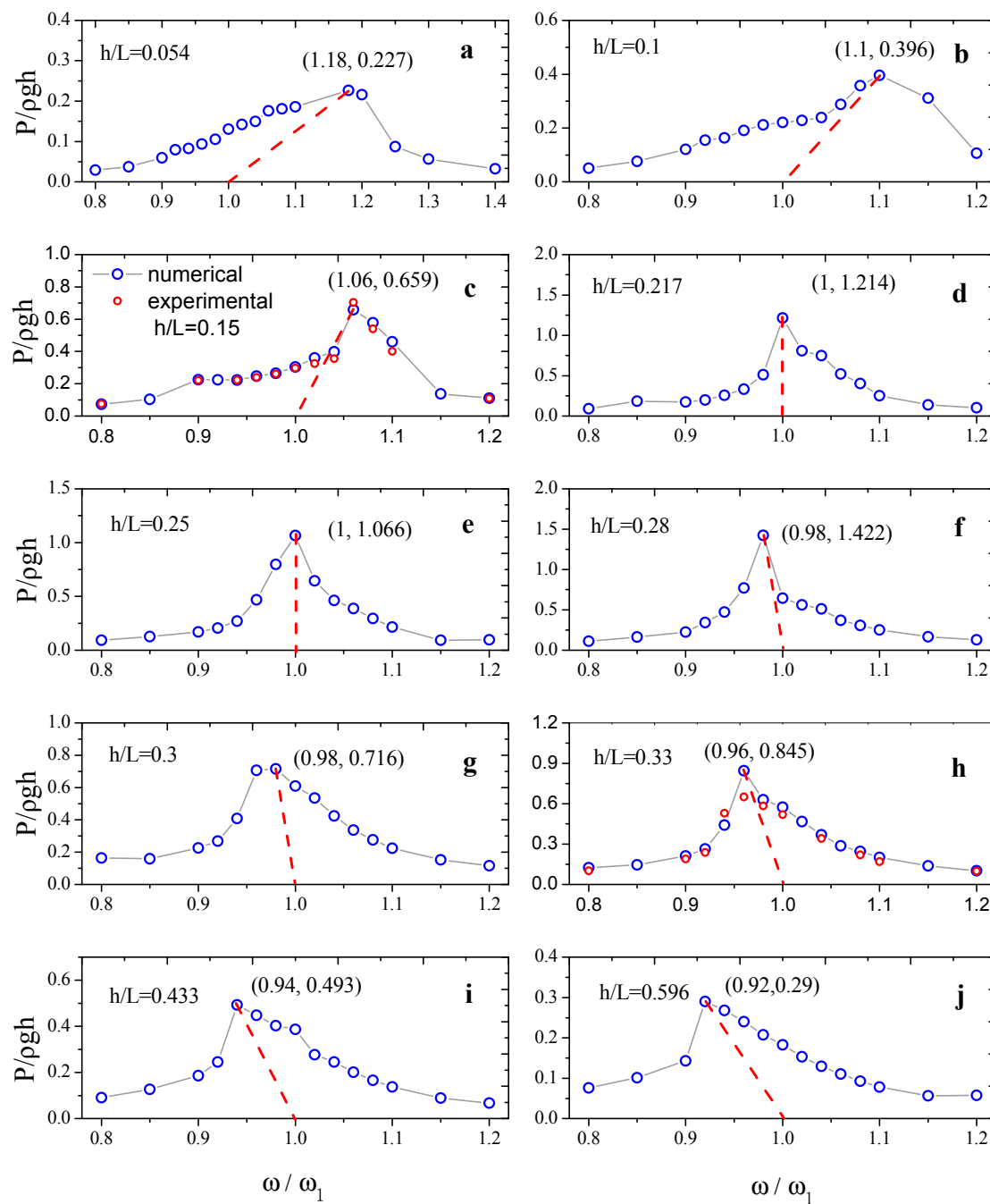
Case	h/L	L(m)	h(m)	A(m)	$\omega_1$ (rad/s)	$\omega$ (rad/s)
Case 13	0.054		0.0324		2.942	
Case 14	0.1		0.06		3.953	
Case 15	0.15		0.09		4.749	
Case 16	0.217		0.1302		5.514	
Case 17	0.25	0.6	0.15	0.007	5.804	$0.8 \omega_1 - 1.2 \omega_1$
Case 18	0.28		0.168		6.023	
Case 19	0.3		0.18		6.15	
Case 20	0.33		0.198		6.316	
Case 21	0.433		0.2598		6.711	
Case 22	0.596		0.3576		6.999	

Figure 16 shows the pressure-frequency response curves at 10 different filling levels. In Figure 16c–h, the corresponding experimental are also included for comparison, which, once again, show good agreements and reinforce the credibility of experimental and numerical models. In all the cases, the pressure increases as the frequency increases and then decreases afterward. However, at different filling levels, the rate of increase/decrease and the maximum response frequency are not the same. It can be clearly seen that when the filling level changes from low to high, the ascending process before the maximum response frequency becomes shorter, and the descending process after that becomes longer, the maximum response frequency (Marked in the Figure 16) decreases from  $1.18 \omega_1$  to  $0.92 \omega_1$  instead of keeping the first-mode natural frequency computed by the potential theory.

As is shown in Figure 16a–c, there are ‘soft-spring’ responses in shallow water sloshing; it is characterized by a rapid decrease after a slow rise to the maximum response value, with the maximum response frequency higher than the natural frequency. Besides, Figure 16h–k show a ‘hard-spring’ response in deepwater sloshing. Its characteristic is a slow descent after a rapid rise to the maximum response value and maximum response frequency is less than natural frequency. There is a critical depth, as shown in Figure 16e, at which level the resonance curve becomes symmetric about the natural frequency, being consistent with the resonance in normal harmonic systems.

The occurrences of the ‘soft-spring’ response and the ‘hard-spring’ response may be mainly caused by the nonlinear effect of wave breaking. In order to study the effect of wave breaking, unbroken cases of shallow water and deepwater are set up. With all other conditions remaining the same, the amplitude was reduced to 0.5 mm to make sure that the free surface is not broken during the whole process of sloshing. Figures 17 and 18 show the pressure-frequency response curve, the mean squared error-frequency response curve, the pressure-time history curve, and the spectral analysis at the maximum response frequency in the case of breaking and non-breaking. It should be noted that when at the same depth but without wave breaking, the phenomenon of resonant hysteresis disappears, and the analysis of the max pressure and mean squared error show a similar trend. It is well known that the double peak phenomenon in the pressure-time history curve under resonance indicates two impacts on the tank wall after the sloshing wave is broken. It can be seen in Figure 17 that the resonant sloshing at the low filling level has broken in the third period of sloshing, far earlier than the resonant sloshing at the high filling level. The Fourier transform in Figures 17 and 18 shows that more multiplications of the natural frequency appear in the wave breaking case and the case at the low filling level, which also shows that the phenomenon of wave breaking, will produce nonlinear

effects and the sloshing at the low filling level has stronger nonlinearity than the sloshing at a high filling level.



**Figure 16.** The pressure–frequency response curves at different filling levels. (a)  $h/L = 0.054$ , (b)  $h/L = 0.1$ , (c)  $h/L = 0.15$ , (d)  $h/L = 0.217$ , (e)  $h/L = 0.25$ , (f)  $h/L = 0.28$ , (g)  $h/L = 0.3$ , (h)  $h/L = 0.33$ , (i)  $h/L = 0.433$ , (j)  $h/L = 0.596$ .

Based on the previous section’s conclusion that the external excitation amplitude has a linear effect on the sloshing pressure, the pressure of the  $A = 0.5$  mm case has been expanded 14 times to compare with the pressure of the  $A = 7$  mm case to investigate how the sloshing state will be if the wave cannot break. As shown in Figure 19, the two curves all coincide before wave breaking, but the difference happened after the waves break. A significant phase advance occurred in the pressure–time history curve of shallow water sloshing, and phase delay appears in the pressure–time history curve of

shallow water sloshing. This result shows that wave breaking will change the period of liquid sloshing in the tank. In the condition of shallow water, the period of the liquid sloshing decrease with wave breaking, the maximum response can be achieved at an external excitation frequency greater than the natural frequency. As for deepwater sloshing, the period of the liquid sloshing goes up with the wave breaking, so the system resonance can be excited at an external excitation frequency lower than the natural frequency. These are the root causes of resonant hysteresis and resonance in advance.

Why does the wave breaking have different effects on shallow water and deepwater sloshing? The hydraulic jump is a common phenomenon in shallow water sloshing; Figure 20 shows the wave propagation process before and after the occurrence of the hydraulic jump in the resonant case. It should be noted that the process of a sloshing wave propagating from the highest point on the right wall to the highest point on the left wall takes 0.71 s before the occurrence of the hydraulic jump, but it becomes 0.67 s after the hydraulic jump happens. One reason for this phenomenon is that the liquid climbing up the wall falls vertically and hits the free surface as shown in Figure 20; this force accelerates the velocity at the free surface of the sloshing wave so that the period of the liquid sloshing decreases. The wavelength of deepwater sloshing is longer, a standing wave phenomenon occurs under the excitation of resonance. Figure 21 shows the complex nonlinear phenomenon in deepwater resonant sloshing. It can be seen that there are obvious roof slamming phenomena and aerification which may dissipate energy during each impact. Besides, a large amount of liquid splashing will reduce the depth of water, which will lead to lower wave speed and a longer period of deepwater sloshing.

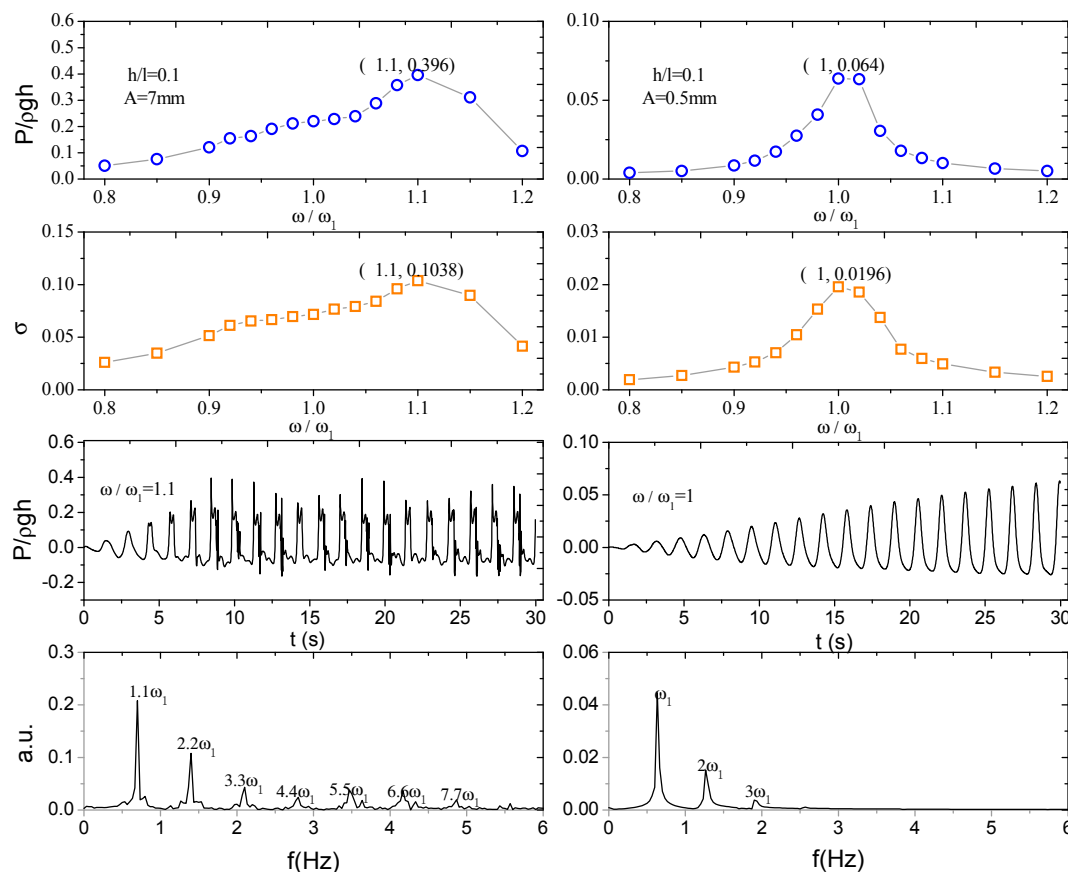


**Figure 17.** The effects of wave breaking on shallow water sloshing. (left column: wave breaking; right column: no wave breaking).



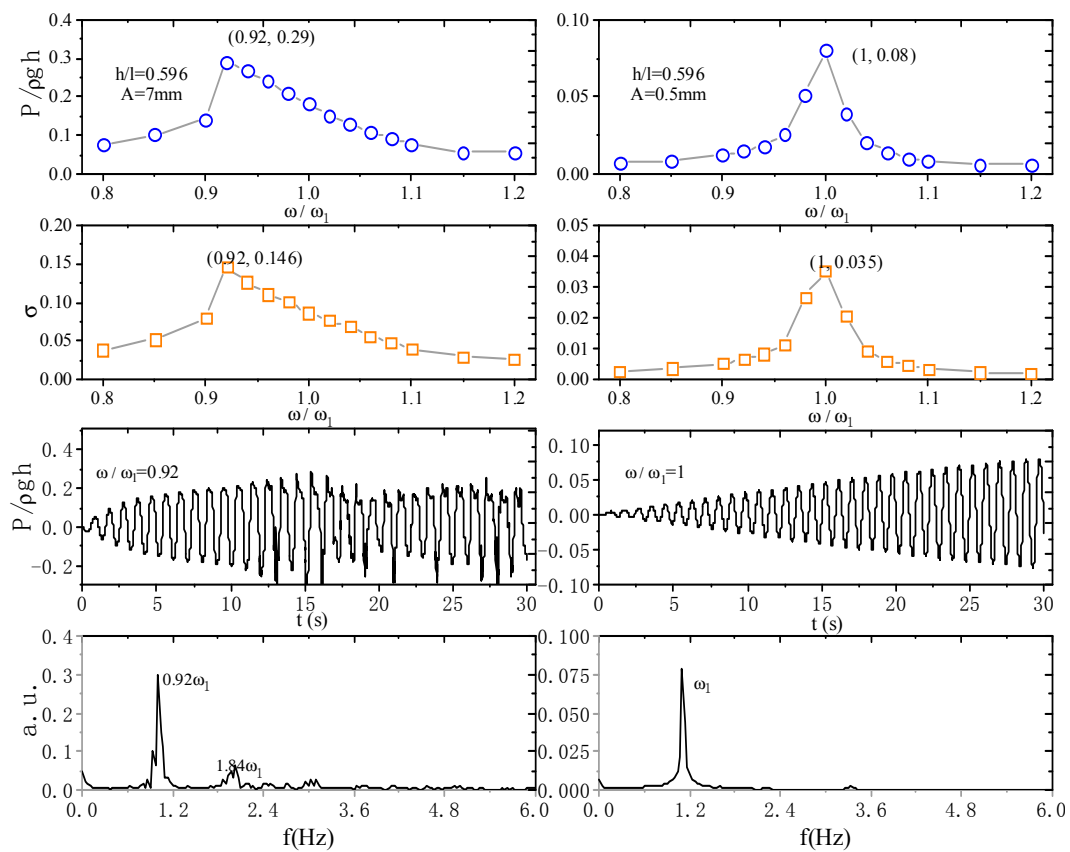


Figure 18. The effects of wave breaking on deepwater sloshing.

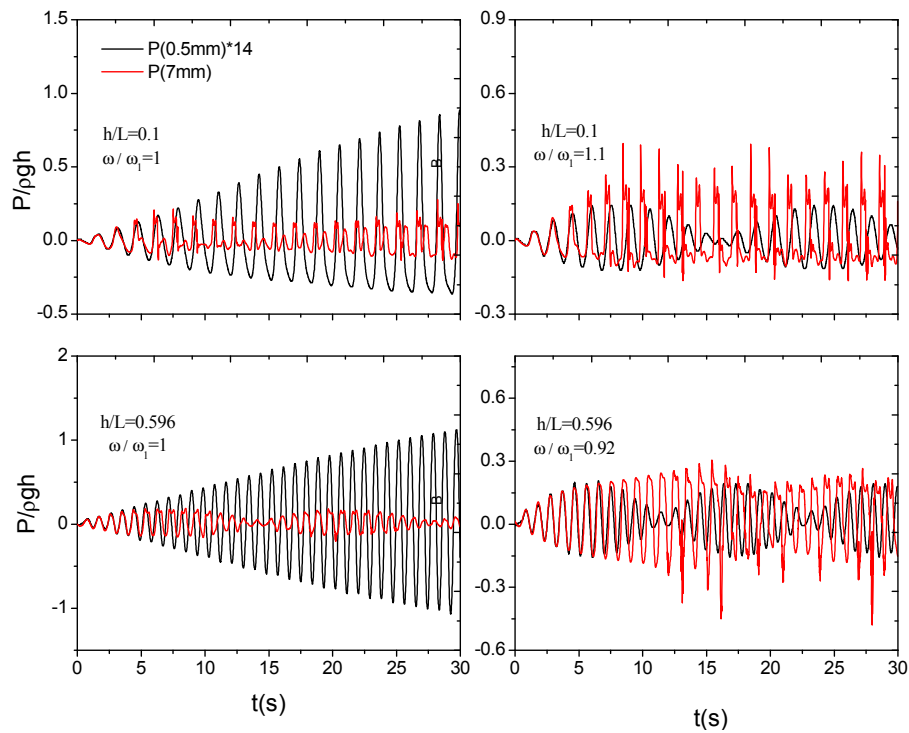
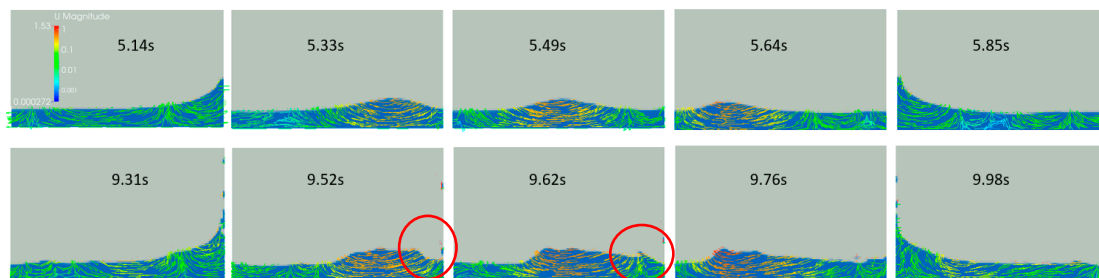
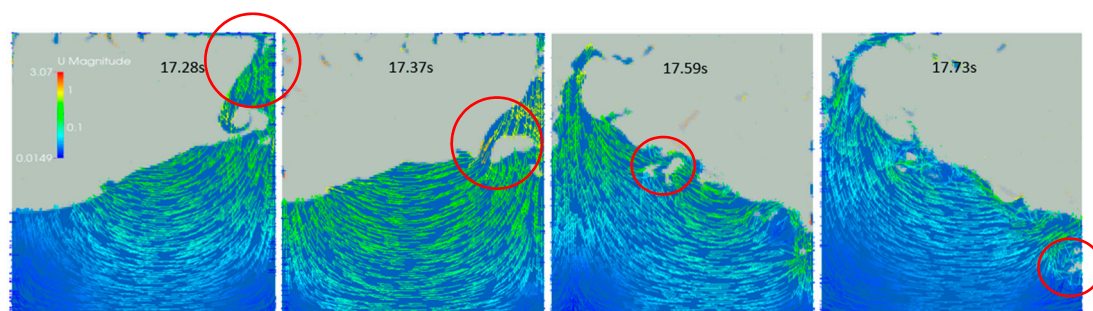


Figure 19. The comparison of pressure-time history curve with wave breaking or not. (red line: wave breaking; black line: no wave breaking).



**Figure 20.** The fluid phenomenon in shallow water sloshing ( $h/L = 0.1$ ,  $\omega/\omega_1 = 1.1$ ,  $A = 7$  mm, the falling liquid hits the free surface in the red circle).



**Figure 21.** The fluid phenomenon in deepwater sloshing ( $h/L = 0.596$ ,  $\omega/\omega_1 = 0.92$ ,  $A = 7$  mm, the phenomena of roof slamming and aerification occurred in the red circle).

## 6. Conclusions

A liquid sloshing numerical model was developed based on OpenFOAM in this study, and a series of experiments were conducted to validate the accuracy of the model. The satisfactory agreement between experimental and numerical data gives support to the assumption that the model is suitable for 2D tank sloshing problems. The numerical results of the 2D model and the 3D model were compared with the experimental results, suggesting an insignificant 3D effect associated with the cases concerned in this paper. Considering the extremely longer Central Processing Unit (CPU) time by the 3D model, the 2D model is preferable and is used in the systematic numerical investigations. A large number of numerical simulations were performed to explore the influence of frequency, amplitude, and the filling level on sloshing: (1) the research on the influence of amplitude indicated that the impact pressure increases as the amplitude grows, and the increase is basically linear in the non-resonance range. Moreover, the change in amplitude affects sloshing more greatly near the resonance frequency. However, under the excitation of resonance frequency, wave breaking may challenge such a principle because of nonlinear effect; (2) the influence of water depth on pressure-frequency response also has been studied, the process of the transition from a 'soft-spring' response to a 'hard-spring' response is observed following the change of the filling level, the ascending trend of the pressures before the maximum response frequency becomes shorter, and the descending process after that becomes longer. The maximum response frequency decreases from  $1.18 \omega_1$  to  $0.92 \omega_1$  moving away from the first-mode natural frequency  $\omega_1$  calculated by potential theory; (3) The main reason for this difference should be the nonlinear effect of wave breaking. The nonlinear effect of wave breaking was studied by a pressure-frequency response curve, the mean squared error-frequency response curve, the pressure-time history curve, and the spectral analysis at the maximum response frequency in the case of breaking and non-breaking. The result show that when at the same depth but without wave breaking, the phenomenon of resonant hysteresis disappears, and the resonance sloshing at a low filling level is more nonlinear than the resonance sloshing at a high filling level; (4) The pressure of the  $A = 0.5$  mm case has been expanded 14 times to compare with the pressure of the  $A = 7$  mm case to investigate how the sloshing state will be if wave cannot break. The result shows that the period of the shallow liquid sloshing decreases with wave breaking, therefore, the maximum response can

be achieved at an external excitation frequency higher than the natural frequency. Combined with the fluid phenomenon in Figures 20 and 21, the reasons may be the liquid climbing up the wall falls vertically and hits the free surface; this force accelerates the velocity of the sloshing wave. In the condition of deep water, the period of the liquid sloshing goes up with wave breaking, so the system resonance can be excited at an external excitation frequency lower than the natural frequency. One reasonable reason is that there is an obvious roof slamming and aerification which may dissipate energy during each slamming. Besides, a large amount of liquid splashing will reduce the depth of the water, which will lead to lower wave speed and a longer period of deepwater sloshing.

Some reasonable reasons have been raised combined with the fluid phenomenon in Figures 20 and 21: (1) the drop of the fluid after the hydraulic jump accelerates the velocity of the sloshing wave; (2) the roof slamming and aerification may dissipate energy during each impact; (3) a large amount of liquid splashing will reduce the depth of water, which will lead to a lower wave speed and a longer period of deepwater sloshing.

**Author Contributions:** Supervision, M.-A.X.; Writing-Original Draft Preparation, Y.C.

**Funding:** This work is supported by the Fundamental Research Funds for the Central Universities (2018B12814), the National Natural Science Foundation of China (51679079), State Key Laboratory of Hydraulic Engineering Simulation and Safety (Tianjin University) (HESS-1703), the Program for Excellent Innovative Talents of Hohai University, the Project to Engage Foreign Experts in Culture and Education of Hohai University (T2018049).

**Conflicts of Interest:** The authors declare no conflict of interest.

## References

- Moiseev, N.N. On the theory of nonlinear vibrations of a liquid of finite volume. *J. Appl. Math. Mech.* **1958**, *22*, 860–872. [\[CrossRef\]](#)
- Faltinsen, O.M. A nonlinear theory of sloshing in rectangular tanks. *J. Ship Res.* **1974**, *18*, 224–241.
- Faltinsen, O.M.; Rognabakke, O.F.; Lukovsky, I.A.; Timokha, A.N. Multidimensional modal analysis of nonlinear sloshing in a rectangular tank with finite water depth. *J. Fluid Mech.* **2000**, *407*, 201–234. [\[CrossRef\]](#)
- Faltinsen, O.M.; Timokha, A.N. An adaptive multimodal approach to nonlinear sloshing in a rectangular tank. *J. Fluid Mech.* **2001**, *432*, 167–200.
- Ikeda, T.; Nakagawa, N. Non-linear vibrations of a structure caused by water sloshing in a rectangular tank. *J. Sound Vib.* **1997**, *201*, 23–41. [\[CrossRef\]](#)
- Pistani, F.; Thiagarajan, K. Experimental measurements and data analysis of the impact pressures in a sloshing experiment. *Ocean Eng.* **2012**, *52*, 60–74. [\[CrossRef\]](#)
- Xue, M.-A.; Zheng, J.; Lin, P.; Yuan, X. Experimental study on vertical baffles of different configurations in suppressing sloshing pressure. *Ocean Eng.* **2017**, *136*, 178–189. [\[CrossRef\]](#)
- Kalinichenko, V.A.; Sekerzh-Zen'kovich, S.Y. Experimental investigation of Faraday waves of maximum height. *Fluid Dyn.* **2007**, *42*, 959–965. [\[CrossRef\]](#)
- Xue, M.-A.; Lin, P.; Zheng, J.H.; Ma, Y.; Yuan, X.; Nguyen, V.T. Effects of perforated baffle on reducing sloshing in rectangular tank: experimental and numerical study. *China Ocean Eng.* **2013**, *27*, 615–628. [\[CrossRef\]](#)
- Cai, Z.H.; Wang, D.Y.; Li, Z. Influence of excitation frequency on slosh-induced impact pressures of liquefied natural gas tanks. *J. Shanghai Jiaotong Univ.* **2011**, *16*, 124–128. [\[CrossRef\]](#)
- Xue, M.-A.; Zheng, J.H.; Lin, P.; Xiao, Z. Violent transient sloshing-wave interaction with a baffle in a three-dimensional numerical tank. *J. Ocean Univ. China* **2017**, *16*, 661–673. [\[CrossRef\]](#)
- Liu, D.; Lin, P. A numerical study of three-dimensional liquid sloshing in tanks. *J. Comput. Phys.* **2008**, *227*, 3921–3939. [\[CrossRef\]](#)
- Buldakov, E. Lagrangian modelling of fluid sloshing in moving tanks. *J. Fluids Struct.* **2014**, *45*, 1–14. [\[CrossRef\]](#)
- Xue, M.-A.; Zheng, J.H.; Lin, P. Numerical simulation of sloshing phenomena in cubic tank with multiple baffles. *J. Appl. Math.* **2012**, *2012*, 1–21. [\[CrossRef\]](#)
- Kim, Y. Numerical simulation of sloshing flows with impact load. *Appl. Ocean Res.* **2001**, *23*, 53–62. [\[CrossRef\]](#)

16. Ramaswamy, B.; Kawahara, M.; Nakayama, T. Lagrangian finite element method for the analysis of two-dimensional sloshing problems. *Int. J. Numer. Methods Fluids* **1986**, *6*, 659–670. [[CrossRef](#)]
17. Oxtoby, O.F.; Malan, A.G.; Heyns, J.A. A computationally efficient 3D finite-volume scheme for violent liquid–gas sloshing. *Int. J. Numer. Methods Fluids* **2015**, *79*, 306–321. [[CrossRef](#)]
18. Kisev, Z.R.; Hu, C.; Kashiwagi, M. Numerical simulation of violent sloshing by a CIP-based method. *J. Mar. Sci. Technol.* **2006**, *11*, 111–122. [[CrossRef](#)]
19. Chen, Z.; Zong, Z.; Li, H.T.; Li, J. An investigation into the pressure on solid walls in 2D sloshing using SPH method. *Ocean Eng.* **2013**, *59*, 129–141. [[CrossRef](#)]
20. Xue, M.-A.; Lin, P. Numerical study of ring baffle effects on reducing violent liquid sloshing. *Comput. Fluids* **2011**, *52*, 116–129. [[CrossRef](#)]
21. Kim, Y. Experimental and numerical analyses of sloshing flows. *J. Eng. Math.* **2007**, *58*, 191–210. [[CrossRef](#)]
22. Jin, X.; Lin, P.Z. Viscous effects on liquid sloshing under external excitations. *Ocean Eng.* **2018**, in press. [[CrossRef](#)]
23. Ma, Z.H.; Causon, D.M.; Qian, L.; Mingham, C.G.; Martinez, F.P. Numerical investigation of air enclosed wave impacts in a depressurised tank. *Ocean Eng.* **2016**, *123*, 15–27. [[CrossRef](#)]
24. Jiang, S.C.; Teng, B.; Bai, W.; Ying, G. Numerical simulation of coupling effect between ship motion and liquid sloshing under wave action. *Ocean Eng.* **2015**, *108*, 140–154. [[CrossRef](#)]
25. Wang, Y.-S.; Politano, M.; Laughery, R. Towards full predictions of temperature dynamics in McNary Dam forebay using OpenFOAM. *Water Sci. Eng.* **2013**, *6*, 317–330.
26. Faltinsen, O.M.; Timokha, A.N. *Sloshing*; Cambridge University Press: Cambridge, UK, 2009.
27. Liu, D.; Tang, W.; Wang, J.; Xue, H.; Wang, K. Comparison of laminar model, RANS, LES and VLES for simulation of liquid sloshing. *Appl. Ocean Res.* **2016**, *59*, 638–649. [[CrossRef](#)]
28. Waterhouse, D.D. Resonant sloshing near a critical depth. *J. Fluid Mech.* **2006**, *281*, 313–318. [[CrossRef](#)]
29. Kobine, J.J. Nonlinear resonant characteristics of shallow fluid layers. *Philos. Trans.* **2008**, *366*, 1331–1346. [[CrossRef](#)] [[PubMed](#)]



© 2018 by the authors. Licensee MDPI, Basel, Switzerland. This article is an open access article distributed under the terms and conditions of the Creative Commons Attribution (CC BY) license (<http://creativecommons.org/licenses/by/4.0/>).